



# Zirconium Doped Precipitated Fe-Based Catalyst for Fischer–Tropsch Synthesis to Light Olefins at Industrially Relevant Conditions

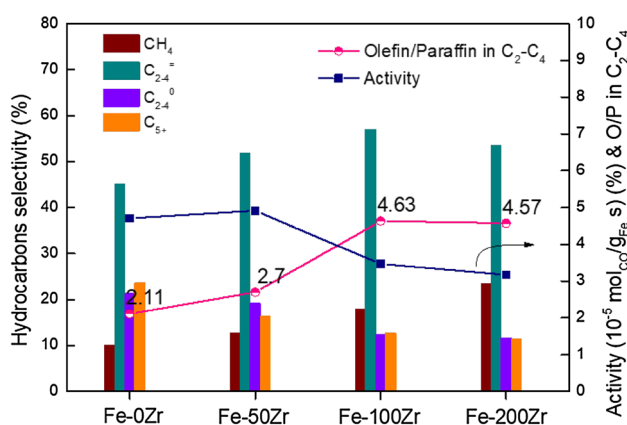
Sanpeng Zhang<sup>1</sup> · Dailin Li<sup>1</sup> · Yi Liu<sup>1</sup> · Yi Zhang<sup>1</sup> · Qing Wu<sup>2</sup>

Received: 28 December 2018 / Accepted: 26 March 2019 / Published online: 3 April 2019  
© Springer Science+Business Media, LLC, part of Springer Nature 2019

## Abstract

Direct conversion of synthesis gas to light olefins (ethylene, propylene, and butylenes) over Fe–Zr co-precipitated catalysts was investigated in a continuous-flow fixed-bed reactor at industrially relevant conditions. The effect of incorporation of zirconium on the textural properties, surface physicochemical properties, and reduction/carburization ability of Fe-based multi-component catalysts were examined by N<sub>2</sub> adsorption–desorption, X-ray diffraction, transmission electron microscope, H<sub>2</sub> temperature-programmed reduction (H<sub>2</sub>-TPR), CO temperature-programmed reduction, and X-ray photoelectron spectroscopy. The results indicated that the addition of less zirconium can promote the dispersion of iron oxide particles and increase the specific surface area of catalyst, leads to a higher Fischer–Tropsch synthesis activity. However, excessive addition of the zirconium promoter will cover the surface active sites and suppress the reduction and carburization of catalyst, which lead to lower activity. Meanwhile, the catalytic stability was destroyed by the addition of less Zr. The charge transfer between Fe and other promoter was redistributed by Zr, which disturbed the original Fe–Mg interaction. When the content of Zr further increased, the stability was improved again by a new formed Fe–Zr interaction. The zirconium promoter can effectively inhibit the chain growth probability and hydrogenation ability, resulting in the improvement of light olefins selectivity.

## Graphical Abstract



**Keywords** Fischer–Tropsch synthesis · Heterogeneous catalysis · Zirconium · Fe-based catalyst · Light olefins

✉ Yi Liu  
yiliu@mail.buct.edu.cn

✉ Yi Zhang  
yizhang@mail.buct.edu.cn

✉ Qing Wu  
wuqing@cnooc.com.cn

Extended author information available on the last page of the article

## 1 Introduction

Fischer–Tropsch synthesis (FTS), which converts syngas (CO and H<sub>2</sub>) derived from coal, natural gas, and biomass into liquid transportation hydrocarbon fuels and value-added chemicals, is of great academic and commercial importance

[1–3]. Light olefins (ethylene, propylene, and butylenes) are important building blocks in chemical industries for the production of polymers, solvents, drugs, cosmetics, and detergents [4]. Traditionally, light olefins are produced by steam cracking of naphtha derived from crude oil, but there is a pressing need for alternative carbon sources and routes in view of the diminishing fossil fuel and environmental issues. Recently, direct synthesis of light olefins from syngas (STO) has become an increasingly important research topic in the conventional FTS process [5–8]. Relative to other FTS catalysts (mainly cobalt-based catalysts), iron-based catalysts are well known for their high selectivity of olefins and low costs. Moreover, it shows a higher resistance to contaminants present in syngas and a higher water–gas shift (WGS) activity allowing for the use of CO-rich syngas derived from coal or biomass. Hence, Fe-containing catalysts are considered to be one of the most adequate catalysts for direct synthesis of light olefins from syngas.

Many different elements have been investigated as possible promoters to improve the light olefins selectivity, activity, and stability such as potassium [7, 9], sodium [6, 10], zinc [10, 11], copper [11, 12], and magnesium [13, 14]. The alkali metal ion ( $K^+$ ,  $Na^+$ ) is expected usually to function as an electronic promoter to affect the electronic state of iron, and can modify the activity and selectivity by enhancing the chemisorption of CO and inhibiting that of  $H_2$  [9, 15]. Promotion of Cu was found to shorten the induction period by accelerating the reduction and carburization of Fe species. In multi-component systems such as co-precipitated Fe–Mn–K catalyst, it was found that Cu could shift the product distribution to heavy hydrocarbons and increase the olefin/paraffin ratio in  $C_2$ – $C_4$  due to the indirect enhancement of surface basicity by the synergistic effect between Cu and K [12]. Magnesium (Mg) is also reported to act as an effective promoter to improve the activity and stability of the catalysts, shift product distribution to lighter molecular weight hydrocarbons and suppress the hydrogenation of light olefins [13, 14].

In addition, some transition metal oxides (Mn, V, Cr, and Zr oxide) are also known to promote the Fe or Co catalyzed FTS reactions [5, 8, 14, 16, 17]. Manganese is the most common promoter for enhancing olefin selectivity while suppressing methane selectivity, by increasing the abundance of adsorbed CO with weakened C–O bonds and accelerating the dissociation of CO [8, 17].  $ZrO_2$  was demonstrated to be a suitable support or support modifier to improve the dispersion of active metal, leads to higher FTS activity and stability on Fe/Co based catalysts [18–24]. Bell et al. [18] reported that Zr promotion effects originate from sites at the Co– $ZrO_2$  interface, which would increase the FTS turnover frequency and the selectivity to  $C_{5+}$  hydrocarbons under FTS conditions. Li et al. [20] investigated the effect of incorporation manner of Zr on the FTS catalytic performance

of Co/SBA-15 catalyst. They found that the addition of Zr improved the turnover frequency (TOF) and promoted the stability of the catalyst. The catalyst prepared by sequential impregnation method (Co/Zr/SBA-15) exhibited the highest selectivity of heavy hydrocarbons ( $C_{12}$ – $C_{22}$ , 53%) due to the high reducibility of cobalt species. Qing et al. [22] prepared a series of Zr-modified Fe/SiO<sub>2</sub> catalysts by precipitation method and found that the Fe–SiO<sub>2</sub> interaction were effectively weakened by  $ZrO_2$ , which consequently enhanced the reduction and carburization of the catalyst and improved the stability of the iron carbides formed. However, Goodwin et al. [16, 23] claimed that the presence of Zr promoters only increased the dispersion of Fe species but did not significantly change the reducibility and hydrocarbon selectivity.

At present, the effects of Zr promoter on catalyst performance remain ambiguous, and few studies have attempted to address the deeper question of whether Zr has any role on the formation of light olefins in traditional FTS conditions. Moreover, in previous reports, little information on the effects of Zr in industrialized co-precipitated Fe-based catalysts was provided. This could be due to the complex nature of the interaction between multifarious metal oxides (such as Fe, Cu, K, Mn) and the support in multi-component catalysts, which makes it difficult to gain more insight into this promotional effect.

In the present work, a series of Fe–Zr co-precipitated catalysts (Fe–Cu–Mn–Mg–Zr) with different Zr content were synthesized by precipitation method and evaluated in a continuous-flow fixed-bed reactor to investigate the effects of Zr on the catalyst performance for FTS under industrially relevant conditions. These obtained catalysts were characterized by  $N_2$  adsorption–desorption, X-ray diffraction (XRD), transmission electron microscope (TEM),  $H_2$  and CO temperature-programmed reduction ( $H_2$ -TPR/CO-TPR), and X-ray photo-electron spectroscopy (XPS).

## 2 Experimental

### 2.1 Catalyst Preparation of Precipitated Fe–Zr Catalysts

The Zr-promoted and Zr-free Fe-based catalysts were prepared by a co-precipitation method. First, the aqueous solution containing  $Fe(NO_3)_3 \cdot 9H_2O$  (99.9%, Tianjing Chemical Co., P. R. China),  $Cu(NO_3)_2 \cdot 3H_2O$  (99.9%, Beijing Chemical Co., P. R. China),  $Mn(NO_3)_2 \cdot 4H_2O$  (Aldrich 99.99%),  $Mg(NO_3)_2 \cdot 6H_2O$  (99.9%, Beijing Chemical Co., P. R. China), and  $ZrO(NO_3)_2 \cdot 2H_2O$  (Aldrich 99.99%) with an Fe/Cu/Mn/Mg/Zr molar ratio of 200/8/50/100/X (X=0, 50, 100, 200) were precipitated at 60 °C using 0.4 mol/L  $K_2CO_3$  (99.9%, Beijing Chemical Co., P. R. China) solution. The precipitant was added drop wise to the mixed nitrate solution

with continuous stirring, while pH was kept at  $8.0 \pm 0.1$  via a digital pH meter. After that, the obtained precipitate was aged at room temperature for 12 h then filtered. Second, the resulting sample was washed 5 times with 60 °C distilled water. Afterwards, the sample was dried at 120 °C for 12 h, then by calcinations at 350 °C for 2 h in the atmosphere of air. These four samples were denoted as Fe–0Zr, Fe–50Zr, Fe–100Zr, and Fe–200Zr. All samples were pressed into pellets (10 MPa), crushed and sieved to retain 20–40 mesh particles for reaction tests.

Furthermore, a reference catalyst without Zr and Mg promoters was prepared by the same method with a composition of 200Fe/8Cu/50Mn, and the sample was denoted as 200Fe–8Cu–50Mn. Another reference catalyst without Fe was prepared by the same method with a composition of 8Cu/50Mn/100 Mg/50Zr, and the sample was denoted as 8Cu–50Mn–100Mg–50Zr.

## 2.2 Catalyst Characterization

The Brunauer–Emmett–Teller (BET) surface area, pore volume, and average pore diameter of the fresh catalysts were obtained via nitrogen physisorption at  $-196$  °C in ASAP 2020 equipment (Micromeritics, USA). Each sample was degassed under vacuum at 90 °C for 1 h and 200 °C for 6 h prior to the measurement. Powder X-ray diffraction (XRD) patterns of all fresh catalysts were recorded on XRD-6000 (Shimadzu, Japan) using Cu K $\alpha$  radiation ( $\lambda = 0.154$  nm), scanning in the  $2\theta$  range 10–90° with a speed of 5° min $^{-1}$  at 40 kV and 30 mA. The size and morphology of the catalysts were characterized by high-resolution transmission electron microscope (HRTEM, JEOL, JEM-2100). The specimen was prepared by ultrasonically suspending the sample in ethanol. A drop of the suspension was deposited on carbon-coated copper grids and dried in air.

X-ray photoelectron spectroscopy (XPS) measurements were conducted with VG Scientific ESCALAB 250 spectrometer equipped with the monochromatized Al K $\alpha$  source ( $h\nu = 1486.6$  eV). The binding energies were calibrated by C 1 s peak of adventitious carbon deposit (284.6 eV).

H $_2$ -temperature programmed reduction (H $_2$ -TPR) experiments were carried out in a quartz tube reactor using 50 mg calcined catalysts. The samples were firstly pretreated by reducing gas (10% H $_2$ /90% Ar) at 100 °C for 1 h with a flow rate of 30 ml/min, and subsequently cooled down to 50 °C. After pretreatment, the temperature was increased from 50 to 800 °C at a rate of 8 °C/min. The effluent of reactor passed through a 5 Å molecular sieve trap to remove produced water, before reaching the thermal conductivity detector (TCD). CO-temperature programmed reduction (CO-TPR) experiments were conducted at same conditions as H $_2$ -TPR, except that the reduction

gas was replaced with 10% CO/90% Ar and no trap was added during the CO reduction process.

## 2.3 Catalyst Evaluation Tests

The FTS reaction was conducted in a continuous-flow fixed-bed stainless steel reactor (8 mm I.D.) at 280 °C, 1 MPa, syngas (CO/H $_2$ /Ar = 47.5/47.5/5), and W/F = 5 g $_{\text{cat}}$  h mol $^{-1}$ . About 0.5 g catalysts (20–40 mesh) mixed with 1.0 g quartz sand was packed in the middle of reactor which was heated in a muffle furnace. The reaction temperature of catalyst bed was monitored by a K-type thermocouple controlled by a PID controller. Flow rates of syngas were controlled by a Brooks 5850 TR Series mass flow controller. Exhaust transfer lines were kept at 150 °C to ensure that no condensation of liquid products occurred in front of the ice trap. Before FTS reaction, the catalysts were in situ reduced by syngas (CO/H $_2$ /Ar = 47.5/47.5/5) for 10 h at atmospheric pressure, 300 °C and W/F = 10 g $_{\text{cat}}$  h mol $^{-1}$ .

The effluent gas was on-line analyzed by gas chromatograph (GC-2014C, Shimadzu) equipped with a thermal conductivity detector (TCD) and flame ionization detector (FID). TCD with an Active Carbon column was used to analyze gaseous products (CO, CO $_2$  and CH $_4$ ) while FID with a Porapak-Q column was used to analyze light hydrocarbons (C $_1$ –C $_5$ ). The composition of liquid-phase products collected in ice trap was off-line analyzed by FID with a silicone SE-30 column. The mass balance of all reactions were calculated, which were almost 95% based on carbon mole. The selectivity to oxygenates was below 2% C-mol and has been excluded from the reported product selectivity.

Catalytic activity, expressed as iron time yield (FTY), was expressed as moles of CO converted per gram of Fe per second. CO conversion was calculated on a carbon-mole basis, as follows:

$$\text{CO Conv.} = \left\{ \left( \frac{\text{CO}_{\text{inlet}} - \text{CO}_{\text{outlet}}}{\text{CO}_{\text{inlet}}} \right) \right\} \times 100\%$$

CO $_2$  selectivity was calculated according to:

$$\text{CO}_2 \text{ selectivity} = \left\{ \frac{\text{CO}_2 \text{ outlet}}{(\text{CO}_{\text{inlet}} - \text{CO}_{\text{outlet}})} \right\} \times 100\%$$

The selectivity of hydrocarbon product (C $_x$ H $_y$ ) in a CO $_2$ -free reaction was obtained according to:

$$\text{C}_x\text{H}_y \text{ selectivity} = \left\{ \frac{(x \times N_{\text{C}_x\text{H}_y})}{\sum (x \times N_{\text{C}_x\text{H}_y})} \right\} \times 100\%,$$

$N_{\text{C}_x\text{H}_y}$  indicated the molar number toward a product with  $x$  carbon atoms.

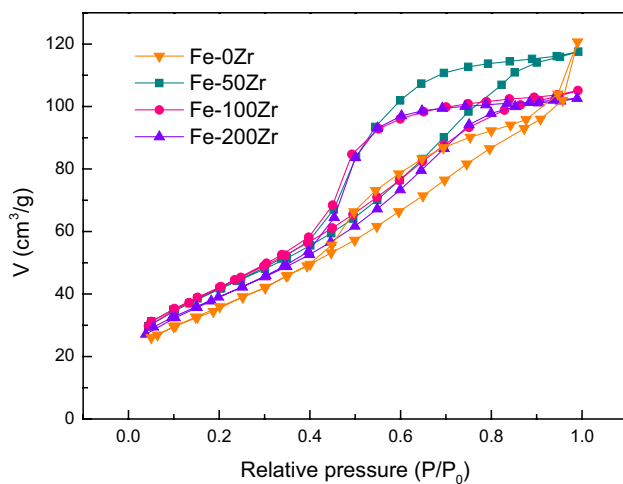


**Fig. 1**  $N_2$  adsorption/desorption isotherms of various Fe–Zr precipitated catalysts as prepared

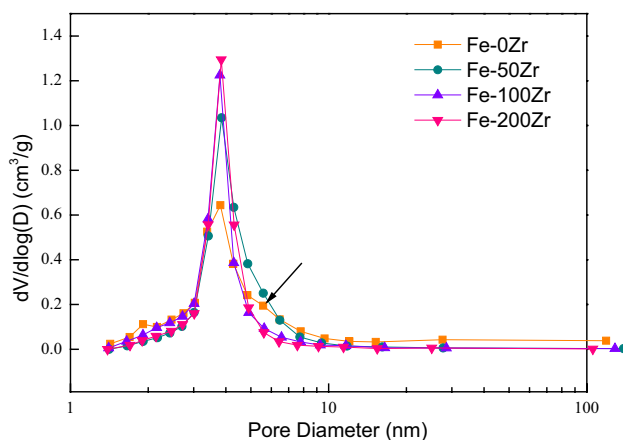


**Fig. 2** Pore-size distributions of various Fe–Zr precipitated catalysts as prepared

## 3 Results and Discussion

### 3.1 Catalysts Characterization

#### 3.1.1 Structural Properties of Fe–Zr Catalysts

The nitrogen adsorption/desorption isotherms and the pore size distributions of the samples Fe–0Zr, Fe–50Zr, Fe–100Zr, and Fe–200Zr are shown in Figs. 1 and 2, respectively. All samples exhibited a type IV isotherm with hysteresis loop, which is typical capillary condensation in the mesoporous materials [24]. Figure 2 indicates narrower pore size distribution in Zr-promoted catalysts than in Zr-free catalyst. For Fe–0Zr sample, it can be found that a shoulder peak appeared at ~6 nm, due to the appearance of larger pores. Information about the texture of the catalysts is presented in Table 1. It is apparent that zirconium influences the BET surface area, pore volume and pore size distribution of iron catalysts. The specific surface area increase from 139  $m^2/g$  for Fe–0Zr sample to 153  $m^2/g$  for Fe–100Zr sample, while further increase in the Zr concentration led to a decrease in specific surface area. Meanwhile, the pore volume monotonously declines with the increase of the zirconium content. Figure 3 shows TEM images of Fe–0Zr and Zr-promoted Fe–100Zr precipitated catalysts as prepared. The images indicate that large (6–10 nm)  $Fe_2O_3$  particles are formed for Fe–0Zr catalyst (Fig. 3a, b), while small particles with sizes less than 5 nm are highly dispersed and distributed homogeneously in Zr-promoted Fe–100Zr sample (Fig. 3c, d). These results strongly suggest that the promotion of zirconium facilitated the dispersion of active crystallites, leads to the decrease of iron oxide crystal size and increase of specific surface area.

To evaluate the effects of Zr on the crystal structure of Fe-based precipitated catalysts, we performed XRD examinations. As shown in Fig. 4, the diffractogram of all Zr-free and Zr promoted Fe-based catalysts only show peaks associated with crystalline  $MnCO_3$  phase (JCPDS 44-1472) at 24.3°, 31.4°, 37.5°, 41.4°, 45.2°, 51.5°, and 51.7°, because these

**Table 1** The textural properties of various Fe–Zr samples as prepared

Catalysts	BET surface area ( $m^2/g$ )	Pore volume ( $cm^3/g$ )	Average pore size (nm) <sup>a</sup>	Average pore size (nm) <sup>b</sup>	Zr/Fe atomic ratio		Binding energy (eV)		
					Stoichiometric	Surface <sup>c</sup>	Fe 2p	Fe 3p	Zr 3d
Fe–0Zr	139	0.21	3.82 (5.58)	4.17	0	0	710.6	55.1	–
Fe–50Zr	150	0.19	3.85	4.12	0.25	0.53	710.7	55.8	181.8
Fe–100Zr	153	0.17	3.80	4.24	0.50	1.00	710.7	55.6	181.9
Fe–200Zr	142	0.17	3.84	4.03	1.00	2.26	710.7	55.5	182.0

<sup>a</sup>Form BJH desorption data

<sup>b</sup>From BJH adsorption data

<sup>c</sup>Determined by XPS analyses of fresh samples



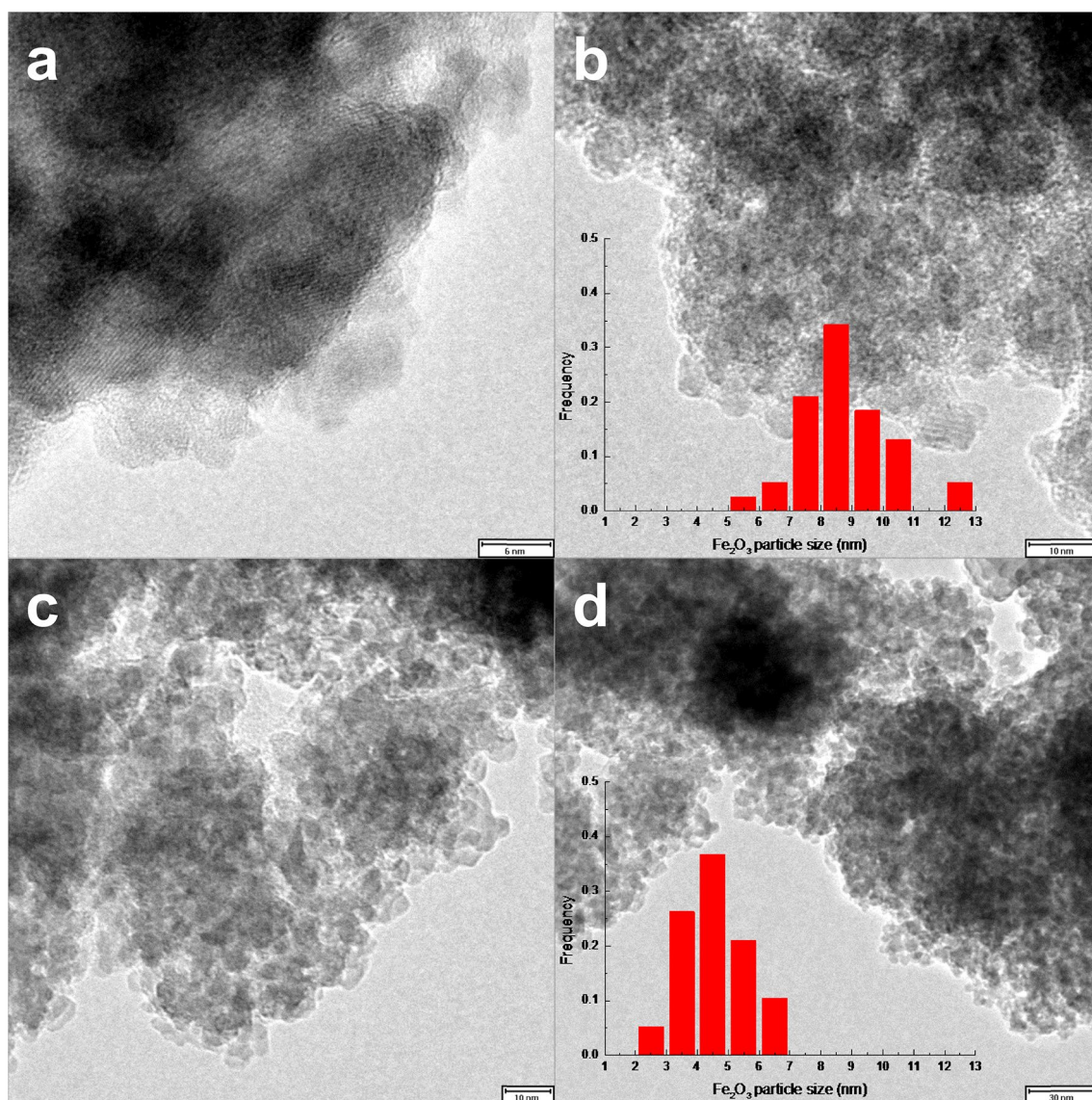


**Fig. 3** TEM images of **a, b** Zr-free Fe–0Zr precipitated catalyst and **c, d** Zr-promoted Fe–100Zr precipitated catalyst as prepared

peaks were also observed for 8Cu–50Mn–100Mg–50Zr and 200Fe–8Cu–50Mn reference samples. No diffraction peaks of Fe oxide phase were observed for all catalysts, and only two broad diffraction regions appeared between  $30^\circ$  and  $40^\circ$ . Such results indicate the Fe oxide species are well dispersed due to the presence of various promoters in this complex multi-component system, as confirmed by TEM. This phenomenon was also reported by other researchers in Fe-based co-precipitated multi-component catalysts [13]. Meanwhile, no characteristic signals of zirconium oxide can be observed in the X-ray diffraction patterns, which imply that zirconium oxide is also well dispersed in the precipitated catalysts.

XPS was used to probe the surface electronic structures of Fe and Zr in all catalysts. Figure 5a–c shows the XPS spectra of the Fe 2p, Zr 3d, and Fe 3p region.

The Fe 2p spectrum (Fig. 5a) of all catalysts display two main peaks attributed to Fe  $2p_{3/2}$  and Fe  $2p_{1/2}$  transitions from Fe<sup>3+</sup> at 710.7 eV and 724.3 eV, suggesting that all of Fe species on the surface of catalyst was present as Fe<sub>2</sub>O<sub>3</sub> phase [25]. The observed spin–orbit doublet peaks in Zr 3d XPS spectra (Fig. 5b) at the binding energy (BE) of  $\sim 181.8$  eV and  $\sim 184.2$  eV correspond to Zr  $3d_{5/2}$  and Zr  $3d_{3/2}$  electrons, which were typical for Zr<sup>4+</sup> in the ZrO<sub>2</sub> phase [26]. We further explored Fe 3p spectra to probe the changes in electronic environment of Fe species in catalysts, as electrons in the outer Fe3p core level are more sensitive to the variation of electronic structures [27]. As shown in Fig. 5c, it can be seen that the binding energy of Fe 3p shift to higher energy (55.8 eV) with the addition of Zr (Fe–50Zr), then decreased gradually with

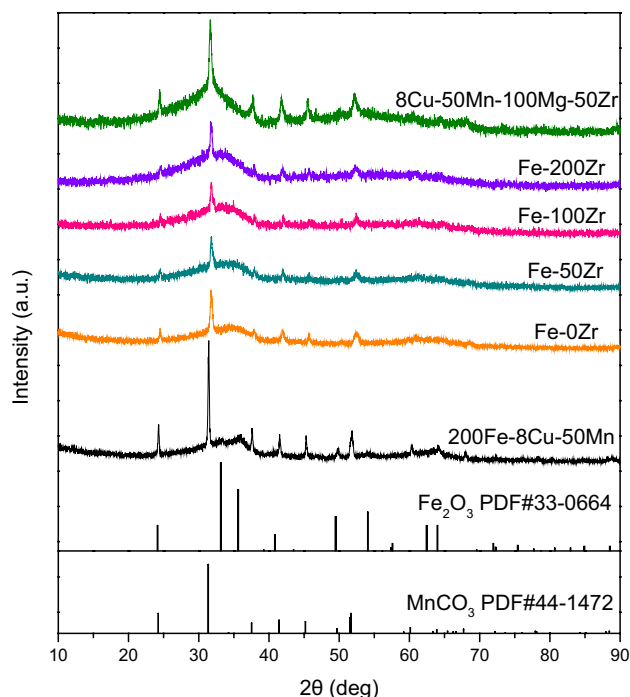


**Fig. 4** XRD patterns of various Fe–Zr precipitated catalysts as prepared

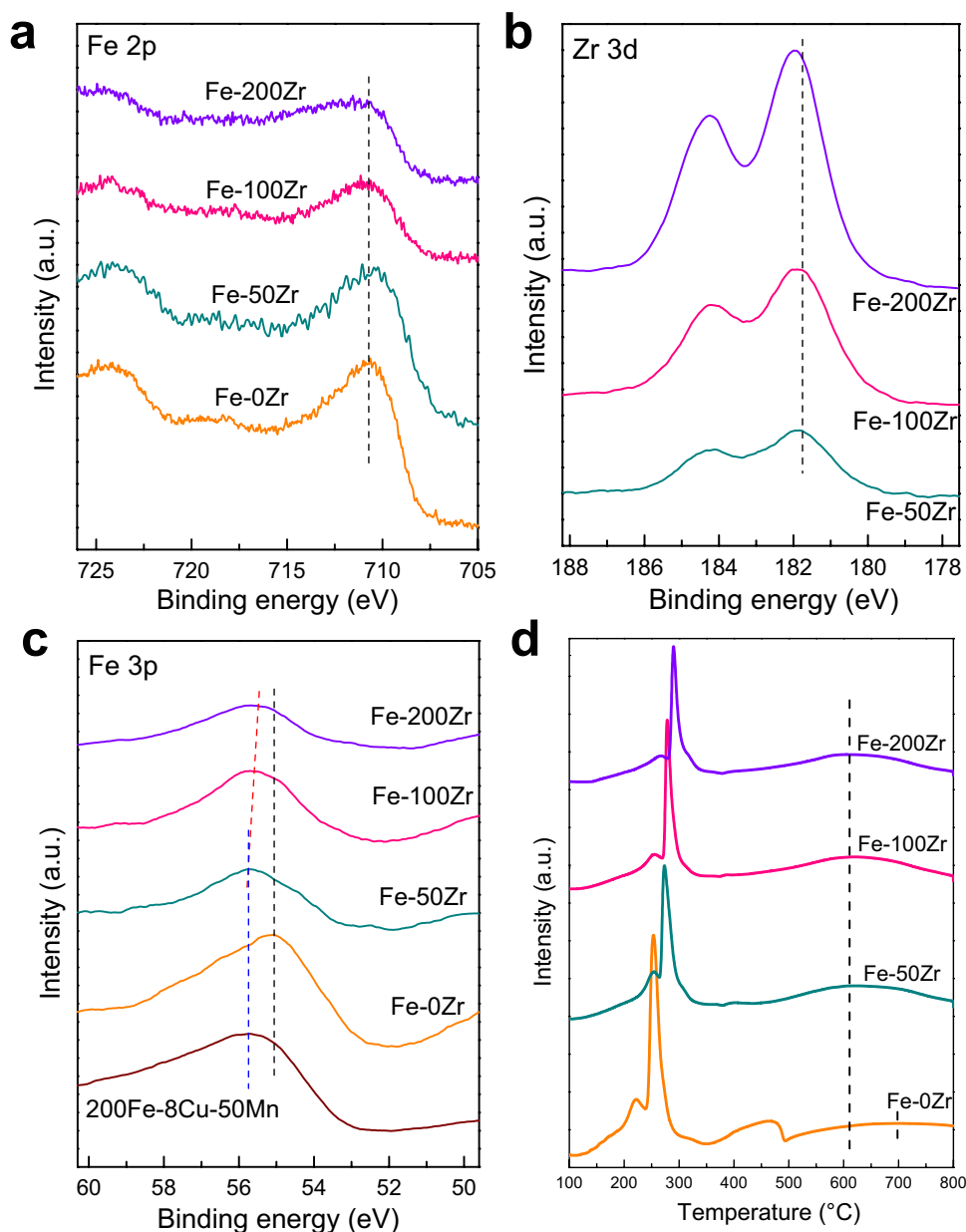
the increase of Zr content. Reasons for this phenomenon cannot be clearly understood due to the complex catalyst composition but may be related to the fact that the charge was redistributed. Considering magnesium has low electronegativity (1.31) and high content (Fe/Mg = 200/100) in this catalyst system, a 200Fe–8Cu–50Mn catalyst without Zr and Mg promoter was further prepared as a reference. As shown in Fig. 5c, the Fe 3p peaks for Fe–0Zr sample shifted to lower binding energy at 55.1 eV compared with that of 200Fe–8Cu–50Mn catalyst at 55.8 eV, indicating a higher electron density of surface Fe species and a strong interaction between iron and magnesium for Fe–0Zr sample. However, this Fe–Mg interaction was disturbed completely when Zr was added, because the binding energy shifts back to higher energy (55.8 eV) for Fe–50Zr sample and was same as 200Fe–8Cu–50Mn catalyst. Furthermore, a little decrease in binding energy of Fe 3p could be observed with increase in Zr content, suggest that a new weak Fe–Zr interaction was present instead of strong Fe–Mg interaction when the Zr content was high enough. If this was the case, the electron density of Zr–O units would decrease, because the electronegativity of  $Zr^{4+}$  (1.33) is lower than that of  $Fe^{3+}$  (1.83). As expected, the presence of Fe–Zr interaction shifted the binding energy of Zr 3d to higher values, especially for the Fe–200Zr sample, as evidenced in Fig. 5b.

### 3.1.2 Reduction and Carburization Behavior of the Fe–Zr Catalysts

In order to further explore the effect of Zr on the reduction behavior of the Fe-based co-precipitated catalysts, the  $H_2$  temperature programmed reduction ( $H_2$ -TPR) results were discussed. As shown in Fig. 5d, the Zr-free Fe–0Zr catalyst exhibited four distinct  $H_2$  consumption peaks with different areas between 200 and 800 °C. According to literature data, the first small peak at 230 °C can be attributed to the reduction of CuO and  $MnCO_3/MnO_x$  to Cu and MnO, and the second sharp peak at 260 °C is ascribed to the reduction of the  $\alpha$ - $Fe_2O_3$  to  $Fe_3O_4$  [12, 28]. The two broad peaks above 450 °C suggest the existence of reduction process of  $Fe_3O_4$ , i.e.,  $Fe_3O_4 \rightarrow Fe$  [12, 22, 28]. For all Zr promoted Fe-based catalysts, the overall TPR profile is obviously narrowed. Reduction for all Zr promoted catalysts starts at a higher temperature and finishes at lower temperature compared with that for the Fe–0Zr catalyst. The profiles clearly show that the first and second reduction peaks of catalysts shifts to higher temperature with the increasing of the zirconium content. This suggests that the addition of the zirconium promoter suppresses the reduction of  $Fe_2O_3$  in  $H_2$  and which results in an increase in the reduction temperature. We proposed that the increase of zirconium content enhances the interaction between  $Fe_2O_3$  and  $ZrO_2$ , and this interaction retards the reduction of  $Fe_2O_3$  during reduction. The  $H_2$ -TPR results provide evidence for the interaction between iron and zirconium to some extent, which is well agreed with XPS result.

The CO-TPR profiles of all catalysts are shown in Fig. 6, which give CO consumption and  $CO_2$  formation rates as a function of temperature. Under CO atmosphere, the reduction and carburization of Fe-based catalysts proceeds in three sequential steps. The first stage at 230–300 °C is probably attributed to the reduction of  $Fe_2O_3$  to  $Fe_3O_4$ ; then,  $Fe_3O_4$  concurrently reduces and carburizes to a mixture of  $Fe_5C_2$  and  $Fe_3C$  at ~400 °C [11]. Above 400 °C, it is clearly observed that the  $CO_2$  formation rate is much lower than CO consumption rate, indicates CO disproportionation occurs via the Boudouard reaction ( $2CO \rightarrow C + CO_2$ ), with the formation of excess amorphous carbon. Furthermore, the comparison between Fe–0Zr and Fe–50Zr samples clearly shows that small amount of zirconium promotes  $Fe_2O_3$  to be carburized due to the much weaker Fe–Mg interaction, resulting in the shift of carburization peaks to the lower temperature. However, further increase of Zr content (Fe–100Zr) leads to the shift of peak to high temperature, due to the formation of a new Fe–Zr interaction. In the case of Fe–200Zr, the shifting of the carburization peak to a much higher temperature compared with that of Fe–0Zr can be ascribed to the difficulty in carburizing  $Fe_3O_4$ , which interact with zirconium with a stronger Fe–Zr interaction when Zr content is high

**Fig. 5** XPS spectra in **a** Fe 2p, **b** Zr 3d, and **c** Fe 3p region from fresh Fe–Zr catalysts. **d** H<sub>2</sub>-TPR spectra of various Fe–Zr precipitated catalysts



enough. This is in good coincidence with the results as indicated by XPS and H<sub>2</sub>-TPR.

### 3.2 Effect of Zirconium on the Catalytic Performance in Fischer–Tropsch Synthesis to Light Olefins

#### 3.2.1 Activity and Stability

The catalytic performances of various Fe-based catalysts with different Zr content in Fischer–Tropsch synthesis were tested at 280 °C, 1 MPa, H<sub>2</sub>/CO ratio of 1, and W/F = 5 g<sub>cat</sub> h mol<sup>-1</sup>. The influence of the zirconium content on activity and stability of the catalysts is shown in Fig. 7. The iron time yield (FTY) of all catalysts increased during the first

5 h of reaction and reached a steady state within 10 h, except Fe–50Zr catalyst and 200Fe–8Cu–50Mn reference sample, which deactivate very rapidly after reach the maximum activity. This result indicates that the addition of Mg could promote the stability of the catalyst, while the inclusion of small amount of zirconium in the catalyst formulation (Fe–50Zr) leads to significant deactivation. According to the characterization results mentioned in foregoing sections, a strong Fe–Mg interaction was present when Mg was added in the catalyst. We proposed that the presence of this strong Fe–Mg interaction can improve the stability by preventing the sintering of the active nanoparticles during the catalytic reaction. However, this interaction was disturbed after the incorporation of small amount of zirconium. Hence, the Fe–50Zr catalyst deactivated with time on stream. When

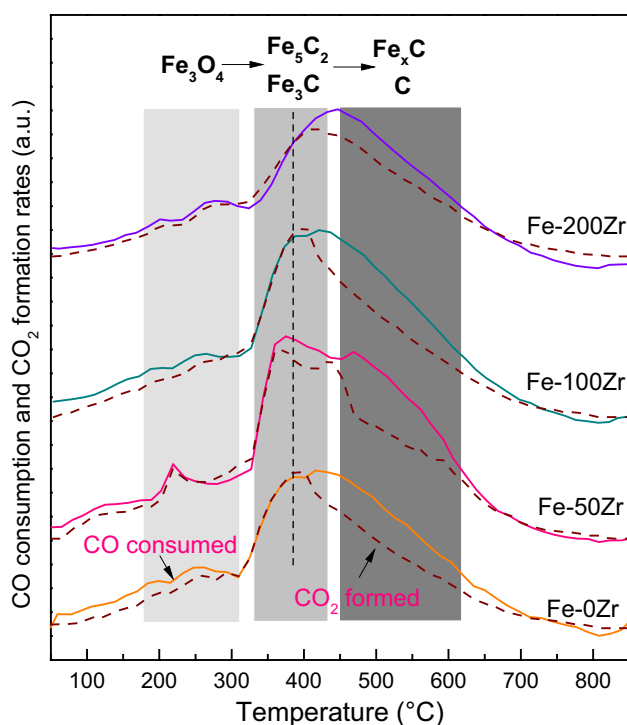


**Fig. 6** Rates of CO consumption and CO<sub>2</sub> formation of Fe–Zr precipitated catalysts during the reduction and carburization in 10%CO/90%Ar

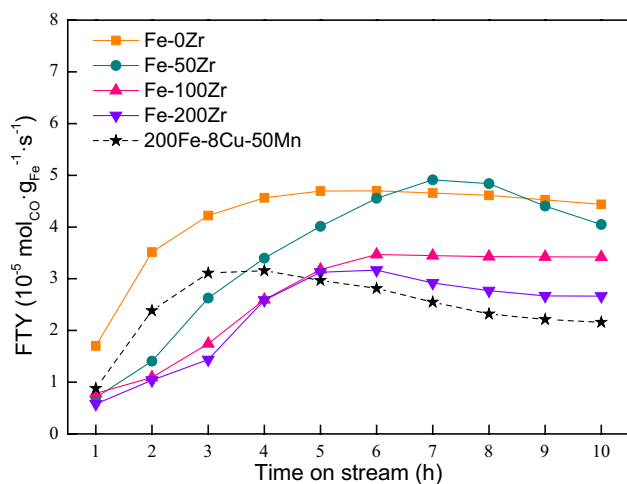


**Fig. 7** Time on stream plot of iron time yield (FTY) of various Fe–Zr catalysts. Reaction conditions: 0.5 g catalyst, H<sub>2</sub>/CO=1, 1 MPa, 280 °C, W/F(CO+H<sub>2</sub>+Ar)=5 g<sub>cat</sub> h mol<sup>-1</sup>

further increase the concentration of zirconium in the Fe-based precipitated catalyst, as in the case of Fe–100Zr and Fe–200Zr, the stability would be improved again due to a newly formed Fe–Zr interaction [29]. At the same time, the stability of the light olefins selectivity for Fe–Zr catalysts was also investigated. Figure 8 shows the plot of light olefins

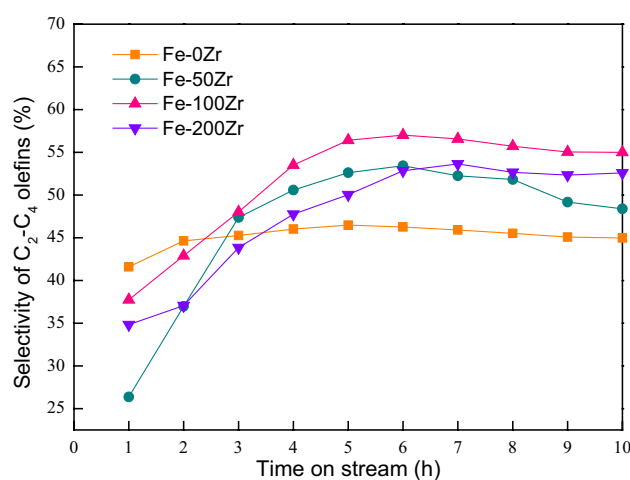


**Fig. 8** Time on stream plot of light olefins (C<sub>2</sub>–C<sub>4</sub>) selectivity of various Fe–Zr catalysts. Reaction conditions: 0.5 g catalyst, H<sub>2</sub>/CO=1, 1 MPa, 280 °C, W/F(CO+H<sub>2</sub>+Ar)=5 g<sub>cat</sub> h mol<sup>-1</sup>

(C<sub>2</sub>–C<sub>4</sub>) selectivity of various Fe–Zr catalysts with time on stream. It is observed that the deactivation only occurred on the Fe–50Zr catalyst. This is similar with the result in activity test curve, in which only Fe–50Zr catalyst deactivates due to the aggregating or sintering of the active nanoparticles.

In addition, it was found that the activity of Fe–50Zr catalyst increased slightly ( $4.91 \times 10^{-5} \text{ mol}_{\text{CO}} \text{ g}_{\text{Fe}}^{-1} \text{ s}^{-1}$ ) compared with Fe–0Zr catalyst ( $4.70 \times 10^{-5} \text{ mol}_{\text{CO}} \text{ g}_{\text{Fe}}^{-1} \text{ s}^{-1}$ ). This can be ascribed to the higher specific surface area of Fe–50Zr catalyst, which exposed more active sites for FTS. However, further increase in the Zr concentration led to a decrease in FTS activity. On the one hand, the reduction and carburization capability of the catalyst (H<sub>2</sub>-TPR and CO-TPR results) was inhibited due to the new formed Fe–Zr interaction, which is responsible for a decrease in the catalyst activity. On the other hand, a decrease in activity could also be a result of the zirconium enriching in the surface and covering iron carbide active sites with the increase of Zr content, as confirmed by XPS (Table 1).

### 3.2.2 Product Selectivity

Figure 9 and Table 2 summarize the product selectivity of various Fe-based catalysts with different Zr content in FTS. The inclusion of zirconium in the catalyst formulation leads to significant changes in the product selectivity. In detail, the methane selectivity increases with increasing the content of zirconium, while the selectivity of heavier hydrocarbons (C<sub>5+</sub>) show an opposite trend to methane. The chain growth probabilities for catalysts with different zirconium content were calculated in carbon number range of C<sub>3</sub>–C<sub>8</sub> and C<sub>10</sub>–C<sub>20</sub> [13]. It can be found that the addition of zirconium suppresses the chain growth ability of catalysts obviously. Compared with Fe–0Zr, the chain growth probability  $\alpha_1$  and



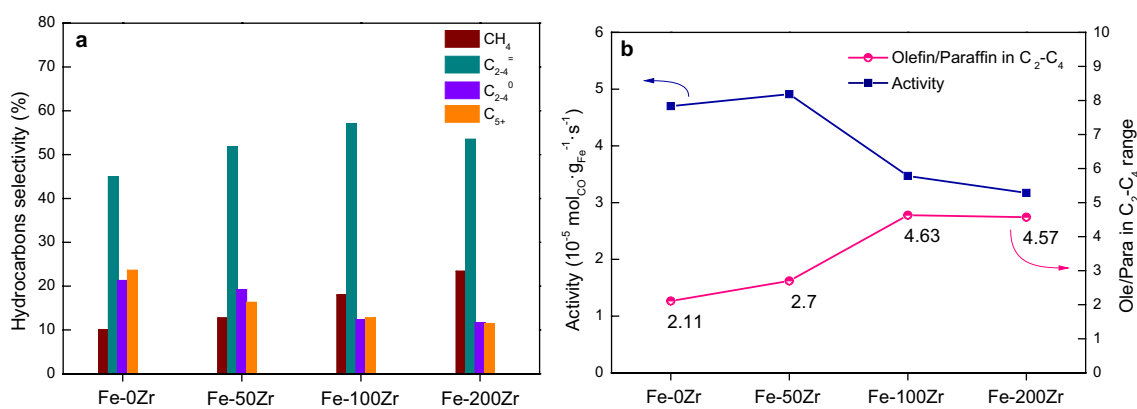


**Fig. 9** The **a** product distribution and **b** activity of various Fe–Zr catalysts for FT synthesis. Reaction conditions: 0.5 g catalyst,  $H_2/CO=1$ , 1 MPa, 280 °C,  $W/F(CO+H_2+Ar)=5 \text{ g}_{\text{cat}} \text{ h mol}^{-1}$

**Table 2** Activity and products selectivities of various Fe–Zr catalysts in fixed-bed Fischer–Tropsch synthesis

Catalysts	FTY ( $10^{-5} \text{ mol}_{\text{CO}} \text{ g}_{\text{Fe}}^{-1} \text{ s}^{-1}$ )	CO Conv. (%)	CO <sub>2</sub> (%CO conv.)	Hydrocarbon selectivity (c-mol%, CO <sub>2</sub> -free)				O/P <sup>a</sup>	$\alpha_1^b$	$\alpha_2^b$
				CH <sub>4</sub>	C <sub>2–4</sub>	C <sub>2–4</sub> <sup>-</sup>	C <sub>5+</sub>			
Fe–0Zr	4.70	86.5	34.3	10.1	45.0	21.3	23.6	2.11	0.52	0.83
Fe–50Zr	4.91	70.3	41.7	12.7	51.8	19.2	16.3	2.70	0.51	0.75
Fe–100Zr	3.47	40.6	39.7	18.0	57.0	12.3	12.7	4.63	0.42	0.68
Fe–200Zr	3.17	27.2	35.1	23.4	53.5	11.7	11.4	4.57	0.39	0.57

Reaction conditions: 0.5 g catalyst,  $H_2/CO=1$ , 1 MPa, 280 °C,  $W/F(CO+H_2+Ar)=5 \text{ g}_{\text{cat}} \text{ h mol}^{-1}$ , TOS 10 h

The data were calculated based on the C-mol percent

<sup>a</sup>The molar ratio of olefin to paraffin in the fraction C<sub>2</sub>–C<sub>4</sub>

<sup>b</sup>The  $\alpha_1$  and  $\alpha_2$  are chain growth probabilities in carbon number ranges of C<sub>3</sub>–C<sub>8</sub> and C<sub>10</sub>–C<sub>20</sub>, respectively

$\alpha_2$  of Fe–50Zr decrease from 0.52 to 0.51 and 0.83 to 0.75, respectively. And it further decreases with the increase of Zr content. The decreased chain-growth probability occurring on the Fe–Zr catalysts might be attributed to the effects of smaller metal particle size [30], as observed in TEM. And we proposed that the lower chain growth probability for Zr-promoted catalysts would be benefit to the formation of light hydrocarbons including light olefins.

Moreover, we also calculated the atomic ratios of Zr/Fe on the surface and in the bulk of calcined catalysts, and the results are listed in Table 1. It was observed that the surface Zr/Fe atomic ratio was higher compared with the bulk compositions, indicating that the surface was enriched with Zr promoter. Hence, the selectivity of light olefins would be improved due to the poor hydrogenation ability of a large amount of ZrO<sub>2</sub> deposited on iron surface [31, 32]. As shown in Fig. 9, the light olefins selectivity increased with increasing Zr content, reaches a maximum at Fe–100Zr catalyst and then decreases slightly. We proposed that the surface Fe<sub>x</sub>C<sub>y</sub> sites of Zr-promoted catalyst can be partitioned into two types of ensembles: region of unpromoted sites that are not close to ZrO<sub>2</sub> and that of promoted sites that are adjacent to ZrO<sub>2</sub>. The volcano-like

evolution of selectivity as a function of amount of loaded Zr suggests that the regions of promoted sites are the interfacial area of Fe<sub>x</sub>C<sub>y</sub> patch with ZrO<sub>2</sub> sites. This assignment is similar to the attribution of active site of WGS catalysis on Cu/CeO<sub>2</sub> to the interfacial area of Cu nanoparticles and CeO<sub>2</sub> [33, 34]. At a relatively low loading, the product selectivity increases along the fraction of the areas of ideal sites (Fe<sub>x</sub>C<sub>y</sub> patch with ZrO<sub>2</sub> sites); further addition of promoter would begin to cover up the iron surface such that reaction performance would decrease simply by there being fewer active sites. The best catalytic performance was obtained on the Fe–100Zr catalyst, which had a relatively high catalytic activity ( $3.47 \times 10^{-5} \text{ mol}_{\text{CO}} \cdot \text{g}_{\text{Fe}}^{-1} \cdot \text{s}^{-1}$ ), higher light olefin selectivity (57.0%) and O/P (olefin/paraffin ratio for C<sub>2</sub>–C<sub>4</sub>) ratio (O/P = 4.63) compared with other catalysts in this work.

## 4 Conclusions

In this work, selective conversion of syngas into light olefins over Zr-promoted Fe-based co-precipitated catalysts was investigated in a continuous-flow fixed-bed reactor at

industrially relevant conditions. The effect of zirconium on chemical/structural properties and catalytic performance of Fe–Zr catalysts was studied. The addition of small amount of zirconium (Fe–50Zr) increased the BET surface area of catalysts and decreased the iron oxide particle size, which leads to a higher activity and lower C–C bond chain growth ability than Fe–0Zr. With further increase of zirconium content, the FTS activity was suppressed due to the surface enriching of Zr promoter, which would cover lots of surface  $Fe_xC_y$  active sites. Meanwhile, a new Fe–Zr interaction was formed and the strength increase with the increase of Zr content. The presence of Fe–Zr interaction can effectively inhibited the sintering of the iron oxide nanoparticles, which gave a stable catalytic performance on Fe–100Zr and Fe–200Zr catalysts. In addition, the surface zirconium species effectively suppress the hydrogenation capacity of primary olefin products, resulting in much higher light olefins selectivity and O/P ratio. Among all the catalysts, the Fe–100Zr catalyst shows a high resistance for catalyst deactivation with highest light olefins selectivity (57.0%) and relatively high CO single pass conversion (40.6%) due to the promotion effects of surface  $ZrO_2$  species.

**Acknowledgment** This work was supported by National Natural Science Foundation of P. R. China (No. 91334206 and 21606011), National “863” program of P. R. China (No. 2013AA031702), and China Postdoctoral Science Foundation (2016M591051 and 2017T100029).

## Compliance with Ethical Standards

**Conflict of interest** The authors declare no competing interest.

## References

- Wender I (1996) *Fuel Process Technol* 48:189
- Dry ME (2002) *Catal Today* 71:227
- Khodakov AY, Chu W, Fongarland P (2007) *Chem Rev* 107:1692
- Galvis HMT, de Jong KP (2013) *ACS Catal* 3:2130
- Zhong LS, Yu F, An YL, Zhao YH, Sun YH, Li ZJ, Lin TJ, Lin YJ, Qi XZ, Dai YY, Gu L, Hu JS, Jin SF, Shen Q, Wang H (2016) *Nature* 538:84
- Galvis HMT, Bitter JH, Khare CB, Ruitenbeek M, Dugulan AI, de Jong KP (2012) *Science* 335:835

## Affiliations

Sanpeng Zhang<sup>1</sup> · Dailin Li<sup>1</sup> · Yi Liu<sup>1</sup> · Yi Zhang<sup>1</sup> · Qing Wu<sup>2</sup>

<sup>1</sup> State Key Laboratory of Organic-Inorganic Composites, Department of Chemical Engineering, Beijing University of Chemical Technology, Beijing 100029, China

- Cheng Y, Lin J, Xu K, Wang H, Yao X, Pei Y, Yan S, Qiao MH, Zong BN (2016) *ACS Catal* 6:389
- Liu Y, Chen JF, Bao J, Zhang Y (2015) *ACS Catal* 5:3905
- Yang Y, Xiang HW, Xu YY, Bai L, Li YW (2004) *Appl Catal A* 266:181
- Zhai P, Xu C, Gao R, Liu X, Li M, Li W, Fu X, Jia C, Xie J, Zhao M, Wang X, Li YW, Zhang QW, Wen XD, Ma D (2016) *Angew Chem Int Ed* 55:9902
- Li S, Li A, Krishnamoorthy S, Iglesia E (2001) *Catal Lett* 77:197
- Zhang CH, Yang Y, Teng BT, Li TZ, Zheng HY, Xiang HW, Li YW (2006) *J Catal* 237:405
- Yang J, Sun Y, Tang Y, Liu Y, Wang H, Tian L, Wang H, Zhang Z, Xiang H, Li YW (2006) *J Mol Catal A* 245:26
- Liu Y, Chen J, Zhang Y (2015) *Reac Kinet Mech Cat* 114:433
- Zhang Q, Kang J, Wang Y (2010) *ChemCatChem* 2:1030
- Lohitharn N, Goodwin JG, Lotero E (2008) *J Catal* 255:104
- Johnson GR, Werner S, Bell AT (2015) *ACS Catal* 5:5888
- Johnson GR, Bell AT (2016) *ACS Catal* 6:100
- Enache DI, Roy-Aubergier M, Revel R (2004) *Appl Catal A* 268:51
- Li Z, Wu J, Yu J, Han D, Wu L, Li J (2016) *J Mol Catal A* 424:384
- Wu YJ, Zhang WT, Yang MM, Zhao YH, Liu ZT, Yan JY (2017) *RSC Adv* 7:24157
- Qing M, Yang Y, Wu B, Xu J, Zhang C, Gao P, Li YW (2011) *J Catal* 279:111
- Lohitharn N, Goodwin JG (2008) *J Catal* 257:142
- Liu Y, Fang K, Chen J, Sun Y (2007) *Green Chem* 9:611
- Cao J, Wang Y, Yu X, Wang S, Wu S, Yuan Z (2008) *Appl Catal B* 79:26
- Kumar S, Kumar S, Tiwari S, Srivastava S, Srivastava M, Yadav BK, Kumar S, Tran TT, Dewan AK, Mulchandani A, Sharma JG, Maji S, Malhotra BD (2015) *Adv Sci* 2:1500048
- Suo H, Wang S, Zhang C, Xu J, Wu B, Yang Y, Xiang H, Li YW (2012) *J Catal* 286:111
- Wan H, Wu B, Xiang H, Li Y (2012) *ACS Catal* 2:1877
- Dang S, Gao P, Liu Z, Chen X, Yang C, Wang H, Zhong L, Li S, Sun Y (2018) *J Catal* 364:382
- Liu Y, Chen JF, Zhang Y (2015) *RSC Adv* 5:29002
- Zhang W, Gao R, Su C, Yin Y (1993) *Stud Surf Sci Catal* 75:2793
- Chen N, Zhang J, Ma Q, Fan S, Zhao T (2016) *RSC Adv* 6:34204
- Graciani J, Mudiyansele K, Xu F, Baber AE, Evans J, Senanayake SD, Stacchiola DJ, Liu P, Hrbek J, Sanz JF, Rodriguez JA (2014) *Science* 345:546
- Park JB, Graciani J, Evans J, Stacchiola D, Senanayake SD, Barrio L, Liu P, Sanz JF, Hrbek J, Rodriguez JA (2010) *J Am Chem Soc* 132:356

**Publisher's Note** Springer Nature remains neutral with regard to jurisdictional claims in published maps and institutional affiliations.

<sup>2</sup> Department of Science & Technology Development, China National Offshore Oil Corporation, Taiyanggong South Street 6, Beijing 100029, China